PAPER

Check for updates

Modeling rapid and selective capture of nNOS–PSD-95 uncouplers from Sanhuang Xiexin decoction by novel molecularly imprinted polymers based on metal–organic frameworks†

Linli Pan,[a] Yingying Ding,[a] Xiaoting Ni,[a] Chong-Zhi Wang,[b] Bo Jiang,[a] Yu Zhang,[a] Nan Jiang,[a] Yulin Tang,[a] Lina Chen [ID] *[a] and Chun-Su Yuan[b]

Novel and highly selective molecularly imprinted polymers based on the surface of metal–organic frameworks, NH_2-MIL-101(Cr) (MIL@MIP$_S$), were successfully fabricated to capture neuronal nitric oxide synthase–postsynaptic density protein-95 (nNOS–PSD-95) uncouplers from Sanhuang Xiexin Decoction (SXD) for stroke treatment. The resultant polymers were characterized by Fourier transform infrared spectroscopy, scanning electron microscopy, thermogravimetric analysis, and X-ray diffraction. The performance tests revealed that MIL@MIPs had a large binding capacity, fast kinetics, and excellent selectivity. Then the obtained polymers were satisfactorily applied to solid-phase extraction coupled with high-performance liquid chromatography to selectively capture nNOS–PSD-95 uncouplers from SXD. Furthermore, the biological activities of components obtained from SXD were evaluated *in vivo* and *in vitro*. As a consequence, the components showed a potent neuroprotective effect from the MTS assay and uncoupling activity from the co-immunoprecipitation experiment. In addition, the anti-ischemic stroke assay *in vivo* was further investigated to determine the effect of reducing infarct size and ameliorating neurological deficit by the active components. Therefore, this present study contributes a valuable new method and new tendency to selectively capture active components for stroke treatment from SXD and other natural medicines.

1. Introduction

Ischemic stroke, characterized by high mortality, a high rate of disability, and high recurrence rate, seriously endangers human health.[1,2] Under the condition of cerebral ischemia, excitatory amino acids are released excessively, causing the over-activation of *N*-methyl-D-aspartate receptor (NMDAR) and the excitation of neuronal nitric oxide synthase (nNOS), which finally results in the over-release of nitric oxide (NO), apoptosis, and nerve damage.[3,4] It was found that blocking the coupling of postsynaptic density protein-95 (PSD-95) and nNOS, downstream of the NMDAR–PSD-95–nNOS signaling pathway, can inhibit the pathological release of NO caused by cerebral ischemia and then cure ischemic stroke without affecting the physiological functions of NMDAR and nNOS.[5–7] IC87201 (ref. 8) and ZL006,[9] small molecule inhibitors of the nNOS–PSD-95 interaction, were developed and reported to have potent neuroprotective activity both *in vivo* and *in vitro*.

[a]School of Pharmacy, Nanjing Medical University, Nanjing, Jiangsu, 211166, China. E-mail: chenlina@njmu.edu.cn; Fax: +86 25 8686 8467; Tel: +86 25 8686 8478

[b]Tang Center for Herbal Medicine Research, Department of Anesthesia & Critical Care, University of Chicago, Chicago, IL 60637, USA

† Electronic supplementary information (ESI) available. See DOI: 10.1039/c9ra10537a

However, considering the strong hydrophilicity and unsatisfactory brain distribution of those small molecules, new nNOS–PSD-95 uncouplers need to be developed urgently.[10]

Natural medicine appears to be an important source to find novel nNOS–PSD-95 uncouplers due to its complex components and excellent neuroprotection, and we had captured potential nNOS–PSD-95 uncouplers such as baicalein (BAI), berberine (BER), and emodin (EMO) from natural medicine[11–13] in our previous work. Sanhuang Xiexin Decoction (SXD), a classic prescription of natural medicine, is composed of Scutellariae Radix (SR), Coptidis Rhizome (CR), and Rhei Rhizome (RR) at a ratio of 1 : 1 : 2.[14,15] Modern pharmacological studies have found that SXD has a lot of bioactivities including anti-inflammatory,[16] anti-oxidative,[17] antidiabetics,[18] anti-hypertension and anti-hyperlipidemia,[19] anti-atherogenic[20] and anti-cerebral ischemia reperfusion injury activities.[21] According to our preliminary experiment, SXD also had obvious uncoupling activity of nNOS–PSD-95. However, it is a time-consuming and laborious task to discover and capture powerful uncouplers from SXD due to its complicated chemical composition. Therefore, a highly sensitive, specific and rapid separation detection method is urgently needed to quickly find nNOS–PSD-95 uncouplers from SXD for anti-stroke applications.

Recently, the developments of molecularly imprinted polymers (MIPs) most likely benefit the study of active components.[22–24] Molecular imprinting technology (MIT), imprinting the template molecule onto a substrate and leaving it with specific recognition sites that match the imprinted molecule in three dimensions,[25] has shown great advantages such as strong resistance to harsh environments, good stability, low cost and easy synthesis, and superior adsorption capacity, and has been applied in natural medicine metabolism analysis,[26] proteins separation,[27] environmental surveillance,[28] immunoassay,[29] biosensors,[30] and simulated enzyme catalysis.[31] Therefore, MIPs can be used as artificial receptors to capture new nNOS–PSD-95 uncouplers.

However, the applications of traditional MIPs are limited by their low adsorption and selectivity, irregular shape, and nonuniform distribution of binding sites.[32] To overcome the above disadvantages, metal–organic frameworks (MOFs) were introduced into the field of MIPs. MOFs are a relatively new type of porous materials with a three-dimensional pore structure that have developed rapidly in recent years, whose surface area is large, porosity is high, structure is regular, and quality is controllable.[33,34] Among which, MIL-101(Cr) has aroused scientific interest for its high chemical and hydrothermal stability, tremendous functional multiplicity, and high specific surface area, which make it an ideal support material.[35,36] Moreover, MIL-101(Cr) was employed as adsorbents for solid phase extraction (SPE) for the determination of sulphonamides in environmental water samples coupling with UPLC-MS/MS.[37] A core–shell MIPs coated onto the surface of MIL-101(Cr) was prepared, which was used as absorbents for the detection of pyrraline in milk and milk powder.[38] NH_2-MIL-101(Cr) was synthesized via a direct hydrothermal method and was coated with polydimethylsiloxane and stir bar for the determination of organophosphorus pesticides in environmental water samples.[39]

Herein, we have prepared highly selective surface molecularly imprinted polymers based on NH_2-MIL-101(Cr) (MIL@MIPs) by molecular imprinting technique (Fig. 1). The characterization, adsorption performance and selectivity capacity were systematically investigated to evaluate the obtained polymers. Then the prepared MIL@MIPs were successfully used as sorbents to quickly discover and efficiently capture potential nNOS–PSD-95 uncouplers from SXD coupled with SPE and HPLC (MIL@MIPs-SPE-HPLC). Finally, SXD and the potential uncouplers captured from SXD were tested with neuroprotective effects on PC12 cells and uncoupling activity by coimmunoprecipitation experiments in vitro. Furthermore, anti-ischemic stroke efficacy was investigated using a reperfusion (MCAO/R) model in vivo.

2. Experimental

2.1 Materials

2-Aminoterephthalic acid (NH_2BDC) and edaravone (EDA) were purchased from Macklin (Shanghai, China). Chromium(III) nitrate nonahydrate ($Cr(NO_3)_3 \cdot 9H_2O$) was obtained from Xilong Scientific Co., Ltd. (Beijing, China). Ultrapure water was produced by the Millipore water purification system (Darmstadt, Germany). Ethylene glycol dimethacrylate (EGDMA), 2,2-azobisisobutyronitrile (AIBN), methacrylic acid (MAA), methyl methacrylate (MMA), 4-vinylpyridine (4-VP), acetonitrile (ACN),

and formic acid of HPLC grade were acquired from Aladdin (Shanghai, China). 2,3,5-Triphenyltetrazolium chloride (TTC) and dimethyl sulfoxide (DMSO) were obtained from Sigma-Aldrich (Steinheim, Germany). 3-(4,5-Dimethylthiazol-2-yl)-5-(3-carboxymethoxyphenyl)-2-(4-sulfophenyl)-2H-tetrazolium, inner salt (MTS) was provided by Promega (Madison, America). ZL006 was provided by Prof. F Li from school of Pharmacy, Nanjing Medical University (Nanjing, China). All the herbal medicines and standards were purchased from Nanjing Yuanbaofeng Pharm-Tech Co., Ltd. (Nanjing, China). All other chemicals used in this paper were of analytical reagent grade.

2.2 Apparatus

A heating magnetic stirrer of C-MAG HS 7 (Staufen, Germany) and an ultrasonic cleaner of KQ-3200B (Jiangsu, China) were applied during the preparation of MIPs. A shake culture box of ZHLY-180 (Shanghai, China) and a centrifugal machine of TG16-WS (Shanghai, China) were used during the elution and adsorption experiment. The optimizing of preparation conditions and evaluation of adsorptive property were conducted by an ultraviolet spectrophotometer of Shimadzu UV-2450 (Kyoto, Japan). The characteristics were carried out with a scanning electron microscopy of FEI Nova Nano SEM 450 (SEM, Hillsboro, USA), a thermogravimetric analyzer of STA449C (TGA, Netzsch, Germany), a Fourier Transform Infrared spectrometer of TENSOR27 (FT-IR, Bruker, Germany), a N_2 adsorption–desorption analyzer of Autosorb-iQ EVO (Quantachrome, USA), and an elemental analyzer of Vario EL III (Elementar, Germany). A HPLC system of LC-20 (Shimadzu, Japan) was used for HPLC analysis and a solid phase extraction apparatus of ASE-12 (Auto Science, China) was used for extraction of target objects.

2.3 Synthesis of NH_2-MIL-101(Cr)

NH_2-MIL-101(Cr) was synthesized according to a previous report with some modifications.[40] $Cr(NO_3)_3 \cdot 9H_2O$ (2 mmol), NH_2BDC (2 mmol), and NaOH (4 mmol) were added to 15 mL deionized water and stirred for 12 min, and then the reaction solution was transferred to a 30 mL Teflon-lined stainless steel autoclave and kept at 150 °C for 12 h. Afterwards, the autoclave was left to naturally cool down to room temperature. Then it was taken out and the green suspension was centrifuged and washed with DMF at room temperature to remove unreacted NH_2BDC for several times and ethanol for 2–3 times. The products were then dispersed into a 50 mL autoclave with 25 mL hot ethanol and kept at 100 °C for 24 h to remove unreacted NH_2BDC in the pores of the product. Finally, the products were taken out and dried at 50 °C for 24 h in a vacuum.

2.4 Preparation of MIL@MIPs

In our previous work, BAI, BER, and EMO were found to have potential uncoupling ability,[11–13] thus they were chosen as templates to synthesize different imprinted polymers (BAI@MIPs, BER@MIPs and EMO@MIPs) respectively, using a surface imprinted polymerization method. Firstly, the template and the functional monomer were dispersed in 40 mL solvent and left to incubate for 4 h at room temperature for self-assembly. Then NH_2-MIL-101(Cr), the cross-
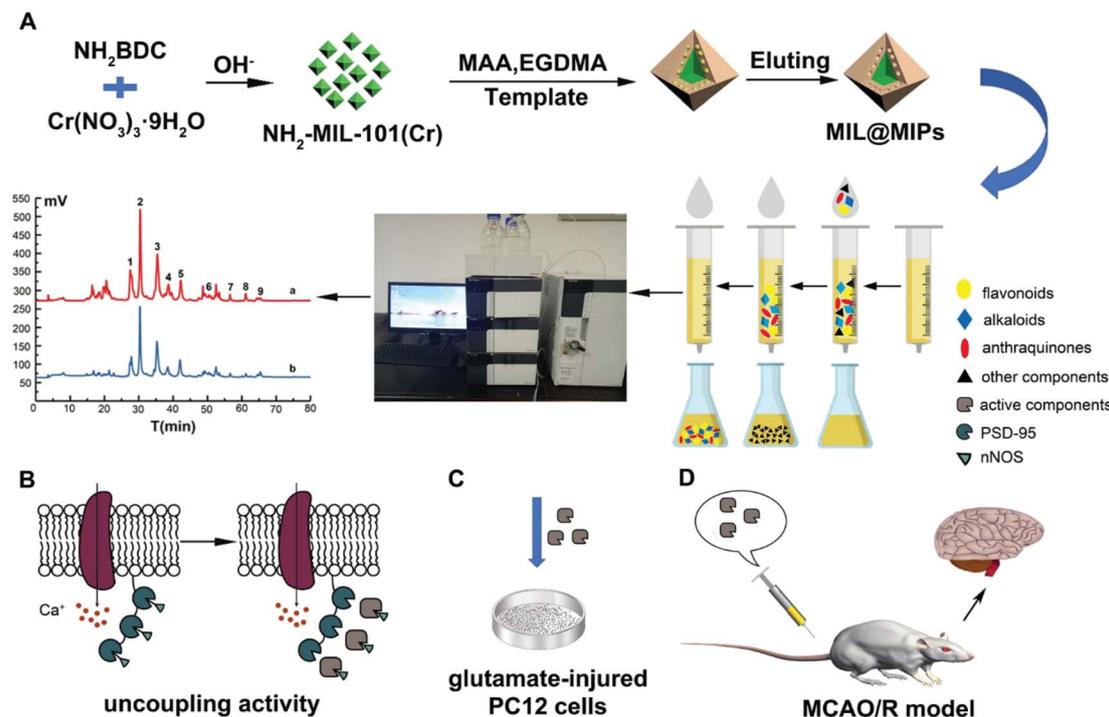
Fig. 1 (A) Schematic illustration for the synthetic process of MIL@MIPs and modeling the MIL@MIPs-SPE-HPLC pretreatment process; (B) the mechanism of uncoupling activity between nNOS and PSD-95; (C) the neuroprotective effects on glutamate-injured PC12 cells of active components *in vitro*; (D) the anti-ischemic stroke effect of active components obtained from SXD *in vivo*.

linker (EGDMA) and the initiator (AIBN) were added and the prepared solution was stirred for 24 h at 60 °C under the protection of nitrogen. After polymerization, the products were repeatedly eluted by methanol–acetic acid (9 : 1, v/v) to absolutely remove templates, and then they were washed with methanol to remove traces of acetic acid until the solution was neutral. Finally, the obtained MIL@MIPs were dried at 50 °C for 24 h in a vacuum. MIL@NIPs were prepared in the same condition just in the absence of templates.

2.5 Evaluation of adsorption performance of MIL@MIPs

To evaluate the adsorption capacity of obtained MIL@MIPs, the static, kinetic, selective, regenerate and reusable adsorption experiments were carried out. All the experiments were conducted for three times in parallel.

For static adsorption experiments, 20 mg MIL@MIPs and MIL@NIPs were respectively suspended in 5 mL EMO, BAI, or BER acetonitrile/ethyl alcohol solution (1 : 2, v/v) with different initial concentrations ranging from 0.5 to 10.0 mmol L^{-1}. The solution was dispersed by being shaken for 2 h and then detected by UV-Vis spectrophotometer. The adsorption amount (Q_e) of polymers was calculated using the following eqn (1):

$$Q_e = \frac{V(C_0 - C_e)}{M} \tag{1}$$

where Q_e represents the equilibrium absorption quantity of templates, C_0 and C_e are the concentration of templates before and after adsorption, respectively, V represents the volume of solution added initially and M is the mass of polymers.

Similarly, for kinetic experiments, 20 mg MIL@MIPs were suspended in 5 mL EMO, BAI, or BER acetonitrile/ethyl alcohol solution with a concentration of 7, 7, or 9, respectively. After that, the solution was shaken under room temperature for a certain interval (5, 10, 15, 20, 25, 30, 40, 50 min).

For selective adsorption experiments, EMO, BAI, BER, and their three structural-liked compounds were assessed, respectively. To investigate the reusability of MIL@MIPs, adsorption–desorption experiments were conducted. The adsorption procedure was the same as described above, and then the MIL@MIPs were eluted with methanol/acetic acid (9 : 1, v/v). After that, the regenerated MIL@MIPs were reused for the next adsorption.

2.6 Purification and capturing nNOS–PSD-95 uncouplers from SXD by MIL@MIPs-SPE-HPLC system

2.6.1 Chromatographic conditions. The HPLC analysis was carried out on a Shimadzu shim-pack C18 column (250 × 4.6 mm, 5 μm). The column temperature was 40 °C and the injection volume was 20 μL with a flow rate of 1.0 mL min^{-1}. The mobile phase consisted of mobile phase A (1% formic acid water) and mobile phase B (acetonitrile). The specific gradient and detection wavelength were described in Table S1.†

2.6.2 Preparation of extracts of SXD. SR (3 g), CR (3 g), and RR (6 g) were powdered to a homogeneous size after being dried, and then they were extracted with 120 mL 90% methanol–water solution by heating reflux at 80 °C for 2 h. The extracts were then filtered and collected for the following use.

2.6.3 Purification and capturing nNOS–PSD-95 uncouplers from SXD. Herein, MIL@MIPs and SPE were combined to capture nNOS–PSD-95 uncouplers from SXD using a MIL@MIPs-SPE column. Firstly, 150 mg EMO@MIPs, 300 mg BAI@MIPs, and 300 mg BER@MIPs were weighed and packed into SPE cartridges. Then, 2.5 mL analysis solution was loaded on the column and left to absorb active components overnight. Afterwards, the column was washed with 5 mL toluene to inhibit nonspecific adsorption at the surface, and then dried thoroughly by a vacuum pump. Subsequently, it was eluted by 10 mL methanol/acetic acid (9 : 1, v/v) to obtain active components. Both the washing and elution solutions were evaporated to dryness by a nitrogen stream at room temperature and the obtained residues were dissolved in 1 mL methanol for further HPLC analysis.

2.7 Activity evaluation of active components obtained from SXD

2.7.1 Neuroprotective effect of active components on PC12 cells. PC12 cells were cultured in DMEM containing 10% (v/v) fetal bovine serum (FBS) and 1% (v/v) penicillin/streptomycin in a 5% CO_2 incubator at 37 °C. To investigate the neuroprotective effect of active components obtained from SXD, the MTS assay was carried out. Firstly, PC12 cells were carefully seeded in 96-well plates (1×10^4 cells per well) and incubated for 24 h. Subsequently, the culture medium was divided into three groups: the blank control group, the glutamate-injured group, and the glutamate-injured group accompanied by ZL006, standards, SXD, or active components of different concentrations (1, 15, 75 and 105 μmol L^{-1}) and held for another 24 h. Then, 20 μL MTS reagents were added to each well and the cells were cultured for another 4 h. During the process, DMSO was applied to dissolve the compounds and the final concentration was less than 0.1% (v/v). A microplate reader was utilized to obtain absorption values at 490 nm and cell viability (%) was calculated by eqn (2):

$$\text{Cell viability (\%)} = \left[\frac{\text{OD}_t - \text{OD}_g}{\text{OD}_c - \text{OD}_g}\right] \times 100\% \qquad (2)$$

where OD_t, OD_g, and OD_c represent the adsorption values of the glutamate-injured group accompanied by the standards, SXD or active components, the glutamate-injured group, and the blank control group, respectively.

2.7.2 Uncoupling activity of active components *in vitro*. Co-immunoprecipitation (Co-IP) was conducted to evaluate the uncoupling activity of active components obtained from SXD. Initially, human embryonal kidney (HEK) 293T cells were cultured in DMEM containing 10% FBS and 50 μg mL^{-1} penicillin/streptomycin in a thermotank until they reached 70–90% fusion degrees. Subsequently, the cells were transfected with pCDH-Flag-nNOS and pcDNA3.1-PSD-95 respectively for 24 h and then were washed with cold phosphate buffer solution (PBS) and lysed with RIPA lysis buffer to obtain a protein solution enriched with Flag-nNOS and PSD-95. Then 120 μL protein A/G immunomagnetic-
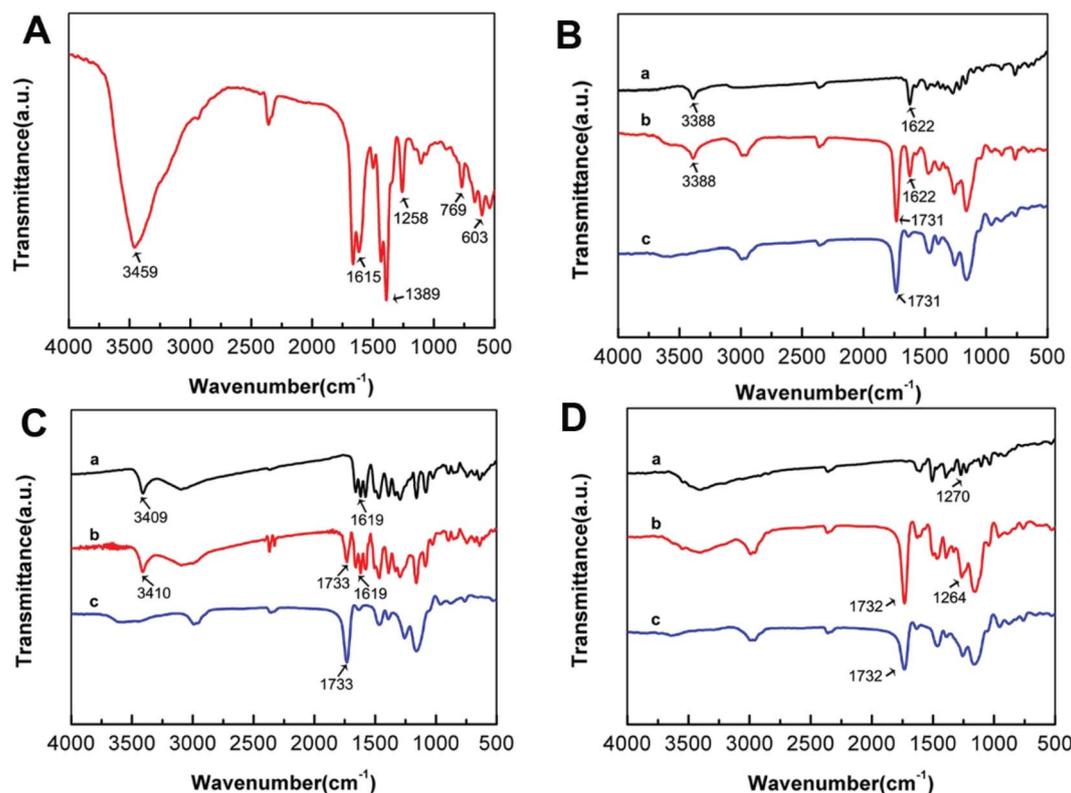

Fig. 2 (A) FT–IR spectrum of NH$_2$-MIL-101(Cr); (B) FT–IR spectrum of (a) EMO, (b) EMO@MIPs before eluting templates, (c) EMO@NIPs; (C) FT–IR spectrum of (a) BAI, (b) BAI@MIPs before eluting templates, (c) BAI@NIPs; (D) FT–IR spectrum of (a) BER, (b) BER@MIPs before eluting templates, (c) BER@NIPs.

beads conjugated with Flag antibody were incubated with the Flag-nNOS protein solution overnight at 4 °C and were incubated with PSD-95 protein solution for 8 h after washing. The complexes were divided into various groups, then added ZL006, standards, SXD, or active components to incubate for another 8 h in 200 μL PBS. Finally, the PSD-95 and Flag-nNOS retained on the beads were analyzed by a western blot.

2.7.3 Anti-ischemic stroke efficacy of active components *in vivo*. In this study, male Sprague-Dawley rats weighting from 240 to 260 g were purchased from the Laboratory Animal Center of Nantong University. The rats were randomly divided into six groups ($n =$ 15): (1) sham-operated group; (2) MCAO group; (3) MCAO + ZL006 (1.5 mg kg^{-1}); (4) MCAO + EDA (6 mg kg^{-1}); (5) MCAO + SXD extracts (23 mg kg^{-1}); (6) MCAO + active components (23 mg kg^{-1}).

The right middle cerebral artery occlusion was operated to induce focal cerebral ischemia with MCAO occlusion line. Briefly, the rats were anesthetized with 10% chloral hydrate (4 mL kg^{-1}) by intraperitoneal injection. Then their right common carotid artery was exposed, and the coated filament was introduced about 20 mm. After 2 h of occlusion, the line was lightly withdrawn and the rats were treated with drugs or 0.9% physiological saline *via* tail vein injection right away. After reperfusion for 24 h, a 5-point neurological function score was employed to evaluate neurological deficit by an observer blinded to the trial. Subsequently, the rats were decapitated and the brains were dissected coronally, and then the slices were immediately stained with 2% TTC solution at 40 °C for 60 min. The stained slices were finally photographed and quantified for ischemic injury by an image assay system. The percentage of infarction was calculated using the following eqn (3):

$$\text{Infarct ratio } (\%) = \frac{\text{Infarct area } (mm^2)}{\text{Half coronal section } (mm^2)} \times 100\% \quad (3)$$

3. Results and discussion

3.1 Optimization the preparation condition of MIL@MIPs

The adsorption ability and selectivity of MIL@MIPs mainly depended on the amount of template, solvent, functional monomer, and the ratio of template/functional monomer/cross-linker. Thus, we prepared different polymers considering of these factors, and the results were shown in Table S2–S4.†

EMO, BAI, and BER were chosen as templates because they were the main components of RR, SR, and CR, respectively. Above all, EMO@MIPs-1, EMO@MIPs-2, and EMO@MIPs-3 were prepared to investigate the effect of the amounts of templates. As shown in Table S2,† EMO@MIPs-2 performed the best adsorption ability when the quantities of NH$_2$-MIL-101(Cr) used were 0.05 g and 0.5 mmol EMO was chosen as the optimal amount of template finally. Solvent plays an important role in preparing EMO@MIPs as well because it is not only the agent to induce holes but also the solvent to distribute the drug evenly. It could be found that EMO@MIPs-2 (acetonitrile/ethanol, 1 : 2, v/v) exhibited the highest adsorption capacity compared with EMO@MIPs-4 and EMO@MIPs-5. EMO@MIPs-4 was prepared

with tetrahydrofuran/ethanol. The polymer was hard and difficult to disperse completely, thus its application was limited.

In addition, a functional monomer was used to self-assemble with template, and three kinds of functional monomers (MAA, MMA and 4-VP) were investigated to obtain the best one. It was shown that the polymers synthesized using MAA had the best adsorption ability. Moreover, we synthesized different polymers with a different ratio of template/functional monomer/cross-linker because it had a great influence on the adsorption properties, and the results showed that the ratio of 1 : 6 : 30 was superior to the others. In conclusion, we found that 0.5 mmol EMO, acetonitrile/ethanol (1 : 2, v/v), MAA, and a ratio of 1 : 6 : 30 were the optimal conditions to synthesize EMO@MIPs. The optimal synthesis conditions and the optimization process of BAI@MIPs and BER@MIPs were exhibited in Table S3 and S4,† respectively.

3.2 Characterization of MIL@MIPs

The FT-IR spectra was detected to demonstrate the successful synthesis of NH$_2$-MIL-101(Cr) and MIL@MIPs. As shown in Fig. 2A, the 3459 cm^{-1} peak was ascribed to the asymmetrical stretching vibration of the amine groups, and the N–H bending vibration was located at 1615 cm^{-1}. Moreover, the peaks at 1389 cm^{-1}, 1258 cm^{-1}, and 769 cm^{-1} corresponded to the C–N stretching vibrations of aromatic amines. Meanwhile, the 603 cm^{-1} was observed, which was attributed to the symmetric stretching of Cr–O. All of the above proved that NH$_2$-MIL-101(Cr) was successfully prepared. EMO@MIPs, BAI@MIPs, and BER@MIPs before eluting templates apparently showed the same characteristic peaks as the templates at 1622 cm^{-1}, 1619 cm^{-1}, and 1270 cm^{-1} as shown in Fig. 2B, C, and D respectively, while they were not found in MIL@NIPs. What's more, the C=O stretching bands at 1731 cm^{-1}, 1733 cm^{-1}, and 1732 cm^{-1} appearing in EMO@MIPs, BAI@MIPs, and BER@MIPs indicated the successful reacting between MAA and EGDMA. All the results demonstrated that MIL@MIPs were successfully made. The TEM and SEM investigations were carried out to exhibit the morphology of NH$_2$-MIL-101(Cr) and MIL@MIPs. From Fig. 3A, we can see that NH$_2$-MIL-101(Cr) showed a uniform size distribution with an average of about 50 nm. The SEM images (Fig. 3B–D) showed that the size of MIL@MIPs increased after the process of encapsulation and the surface was rough, which had various amounts of imprinting cavities.

To evaluate the thermostability of NH$_2$-MIL-101(Cr) and MIL@MIPs, TGA was performed under a temperature of 40 °C to 700 °C. As seen in Fig. 4A (red), there were two obvious weight loss times during the whole process, and the first loss below 180 °C can be mainly attributed to the volatilization of residual solvent, and moisture was about 13%, whereas the other weight loss in a temperature ranging from 200 °C to 600 °C was about 37%, which principally resulted from the structural collapse. From the other three lines in Fig. 4A, we can see that there was a slight decline of about 6% below 300 °C, which was assigned to the elimination of water and residual solvent, and the loss of MIL@MIPs below 700 °C was mainly contributed to the decomposition of the imprinted layer. To further demonstrate the successful coating of the imprinted layer, the XRD patterns were employed. As shown in Fig. 4B, the pattern of NH$_2$-MIL-
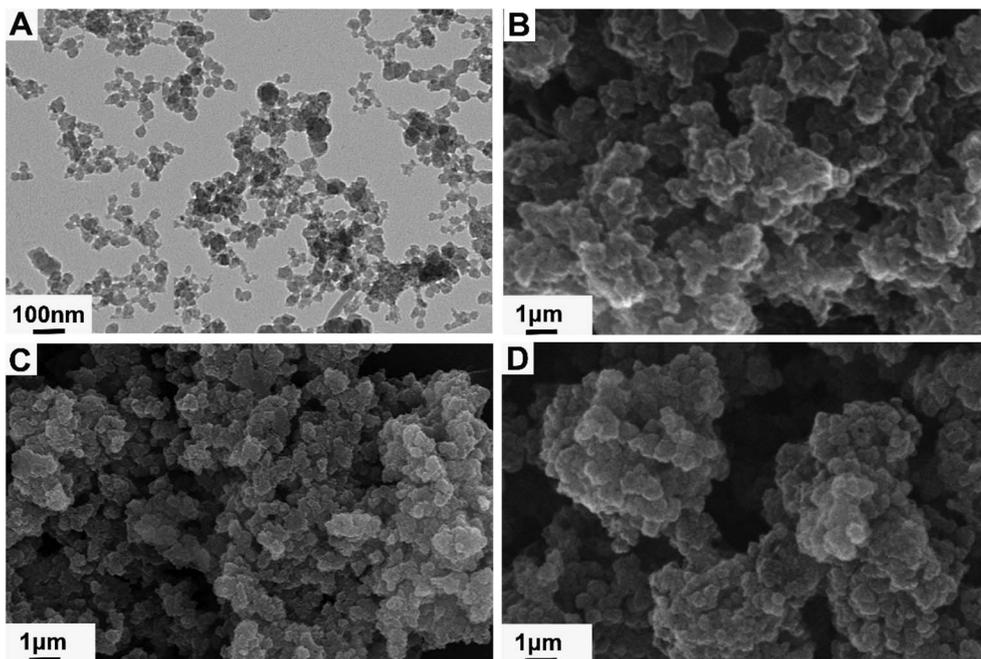
Fig. 3 TEM images of (A) NH$_2$-MIL-101(Cr); SEM images of (B) EMO@MIPs, (C) BAI@MIPs, and (D) BER@MIPs.

101(Cr) was similar to the report in literature[39] and the decline of the patterns of MIL@MIPs also indentified the successful grafting of the imprinted layer.

The elemental analysis of NH$_2$-MIL-101(Cr) and MIL@MIPs was carried out using XPS and the results were shown in Table 1. As we can see, the amount of chromium in MIL@MIPs decreased considerably compared with that of NH$_2$-MIL-101(Cr), and the amount of carbon and protium increased significantly, which demonstrated the successful encapsulation greatly.

The N$_2$ adsorption–desorption measurement was performed to determine the porosity features of NH$_2$-MIL-101(Cr) and MIL@-MIPs, and the results were shown in Table 2. The obtained NH$_2$-MIL-101(Cr) showed obvious large surface area (918.3 m^2 g^{-1}) and pore volume (0.721 cm^3 g^{-1}), which greatly improved the efficiency of MIL@MIPs. With the occurrence of imprinting, the BET surface area and pore volume of MIL@MIPs decreased, which could also

identify the successful encapsulation of MIL@MIPs on the surface of NH$_2$-MIL-101(Cr).

3.3 Adsorption performance of MIL@MIPs

Static adsorption experiments were conducted to evaluate the adsorption ability of MIL@MIPs and MIL@NIPs using the initial

Table 1 XPS analysis of elemental composition (atom%) for synthesized nanoparticles

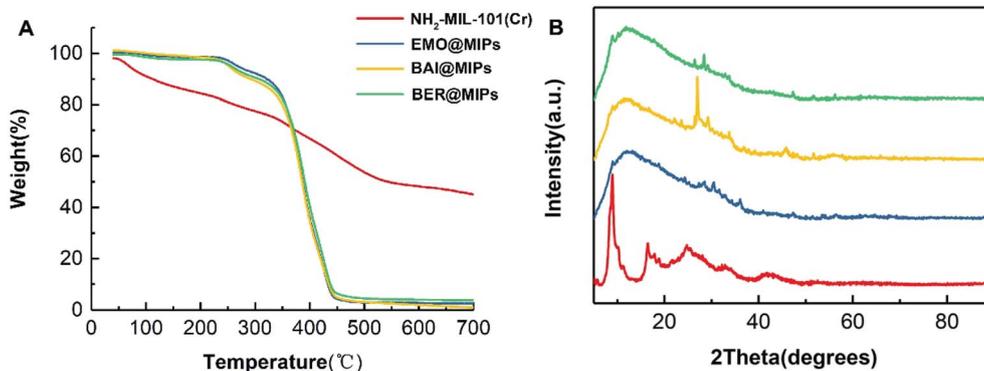|	Cr	C	N	H
NH$_2$-MIL-101(Cr)	9.41	29.19	4.81	4.85
EMO@MIPs	0.16	55.28	<0.3	7.23
BAI@MIPs	0.19	57.25	<0.3	7.32
BER@MIPs	0.28	57.07	<0.3	7.24

Fig. 4 (A) Thermogravimetric weight loss curve of (red) NH$_2$-MIL-101(Cr); (blue) EMO@MIPs; (yellow) BAI@MIPs; (green) BER@MIPs; (B) the XRD of (red) NH$_2$-MIL-101(Cr); (blue) EMO@MIPs; (yellow) BAI@MIPs; (green) BER@MIPs.

Table 2 N₂ adsorption/desorption analysis for various samples

	S_{BET} (m² g⁻¹)	V_t (cm³ g⁻¹)
NH₂-MIL-101(Cr)	918.3	0.721
EMO@MIPs	144.18	0.092
BAI@MIPs	175.7	0.214
BER@MIPs	294.6	0.273

concentration of 0.5–10 mmol L⁻¹. From Fig. S1,† we can see that MIL@MIPs showed a rising trend of binding capacity until the initial template concentration was about 7, 7, and 9 mmol L⁻¹ for EMO, BAI, and BER respectively, and the saturated adsorption capacity was 108.54 µmol g⁻¹, 81.52 µmol g⁻¹, and 114.46 µmol g⁻¹ severally. However, MIL@NIPs showed much lower adsorption amounts, nearly less than half of MIL@MIPs, which was mainly attributed to its nonspecific binding.

Kinetic adsorption curves were used to illustrate the mass transfer property of MIL@MIPs at different time intervals of 5–50 min, and the results were shown in Fig. S2.† The adsorption ability reached equilibrium at the time of 40, 30 and 30 min respectively for EMO@MIPs, BAI@MIPs, and BER@MIPs, and the rapid adsorption property was primarily ascribed to the specific imprinting sites of templates, because of which, the templates could reach the imprinting cavities easily and quickly.

Selective adsorption experiments were performed to estimate the specificity recognition capacity of MIL@MIPs and MIL@NIPs. Fig. S3† clearly indicated that MIL@MIPs showed better binding capacity to the template than its structural analogues, which was owed to the specific recognition sites encapsulated on the surface of MIL@MIPs previously. Nevertheless, MIL@NIPs showed no obvious difference in binding capacity to both the template and its structural analogues, which suggested that MIL@NIPs had no specificity recognition capacity but physical adsorption.

Subsequently, desorption experiments and reusability were detected because regeneration and reusability play an important role in the application of MIL@MIPs. As shown in Fig. S4,† the desorption efficiency reached equilibrium quickly at the

Table 3 The linear regression and performance characteristics of the developed method

| Analyte	Linear regression date			RSD (%)			
	Regression equation	R^2	Test range (mg mL⁻¹)	Intra-day	Inter-day	LOD (µg mL⁻¹)	LOQ (µg mL⁻¹)
Coptisine	$y = 50\,849\,668x - 173\,567$	0.9999	0.001–1.0	1.7	2.2	0.02	0.36
Baicalin	$y = 47\,920\,753x - 34\,619$	0.9998	0.001–0.5	1.1	1.8	0.06	0.33
Berberine	$y = 53\,235\,032x - 31\,678$	0.9995	0.01–1.0	1.3	1.0	0.09	0.32
Emodin-8-O-β-D-glucoside	$y = 30\,475\,821x - 31\,351$	0.9998	0.001–0.5	2.1	1.6	0.08	0.48
Wogonoside	$y = 56\,404\,870x + 27\,287$	0.9999	0.001–1.0	2.3	1.2	0.08	0.33
Baicalein	$y = 50\,389\,185x + 390\,926$	0.9996	0.01–1.0	3.1	2.4	0.13	0.28
Emodin	$y = 48\,624\,763x + 118\,102$	0.9997	0.01–1.0	1.9	2.0	0.06	0.12
Chrysophanol	$y = 90\,029\,676x + 56\,580$	0.9998	0.001–0.3	1.2	1.8	0.02	0.54
Physcion	$y = 16\,807\,416x - 5875$	0.9999	0.001–0.2	3.2	2.9	0.07	0.45
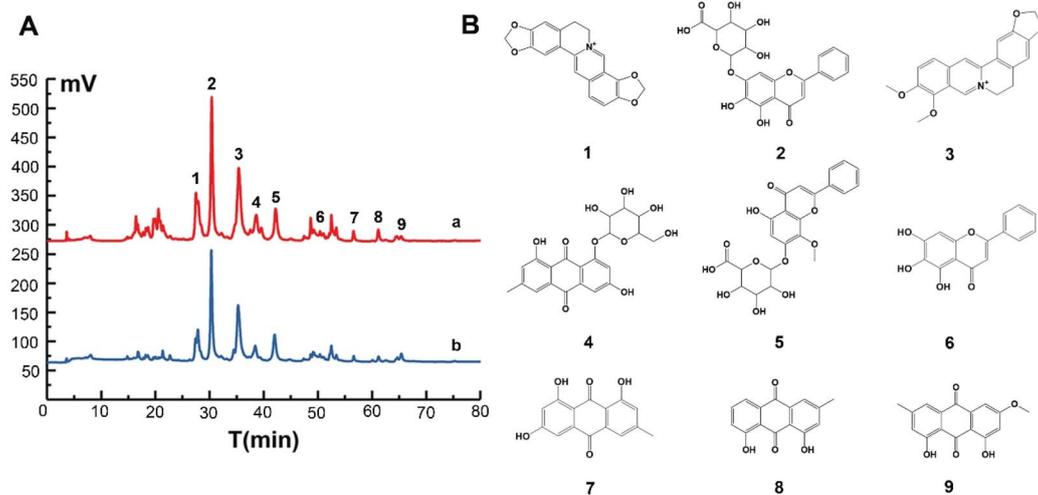
Fig. 5 (A) Chromatograms of SXD extract before (a) and after (b) treatment with MIL@MIPs; (B) structures of the compounds obtained: (1) coptisine, (2) baicalin, (3) berberine, (4) emodin-8-O-β-D-glucopyranoside, (5) wogonoside, (6) baicalein, (7) emodin, (8) chrysophanol, (9) physcion.
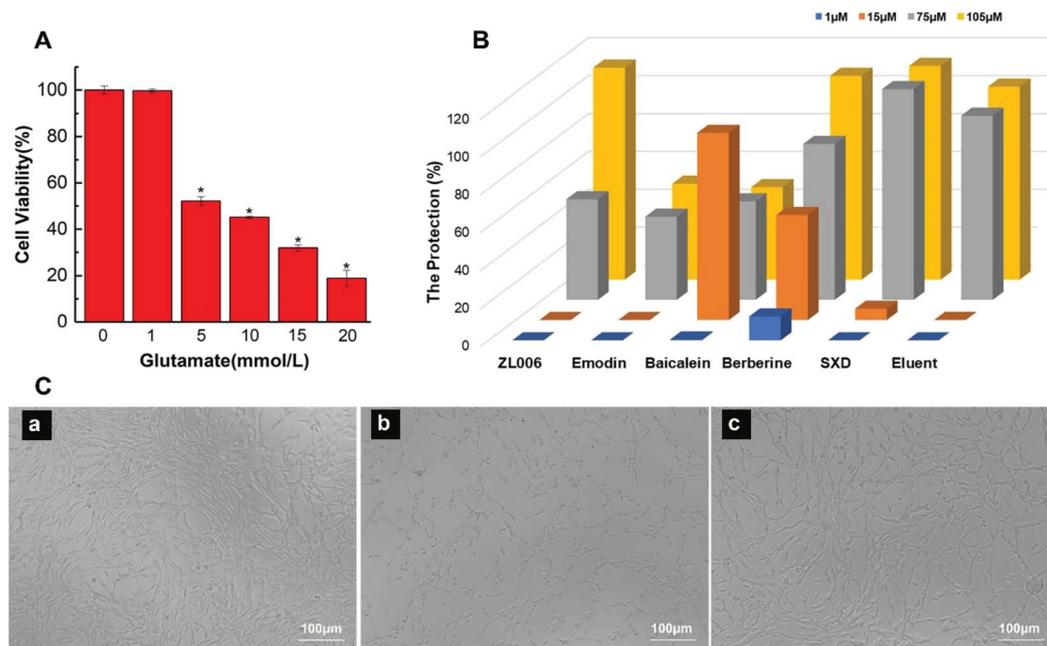
Fig. 6 (A) Cell viability of PC12 with treatment of different concentrations of glutamate; (B) neuroprotective effects on glutamate-injured PC12 cells of ZL006, emodin, baicalein, berberine, SXD and eluent (active components); (C) the control cells (a), 5 mmol L^{-1} glutamate-injured cells (b), cells treated with 5 mmol L^{-1} glutamate and 105 μmol L^{-1} active components (c). Date is presented as mean ± S.D. *$p < 0.05$ compared with the control.

time of 10, 20, and 10 min for EMO@MIPs, BAI@MIPs, and BER@MIPs respectively, which was mainly due to the specific binding site and fast mass transfer property. After that, the regenerated polymers were reused for adsorption and the consecutive adsorption–desorption process was repeated with the same MIL@MIPs for six times. Fig. S5† showed that the binding capacity of MIL@MIPs decreased slowly, which highly indicated that the MIL@MIPs were stable and reusable and could be used for the following adsorption experiments.

3.4 Application

3.4.1 Methodology validation. The optimized method of MIL@MIPs-SPE-HPLC was seriously validated including linear range, correlation coefficient (R^2), limit of detection (LOD), limit of quantification (LOQ), and precisions of intra-day and inter-day. As shown in Table 3, the linearity was very good with the linear range of 0.001–1.0 mg mL^{-1} and R^2 of 0.9995–0.9999. The LOD and LOQ were 0.02–0.13 μg mL^{-1} and 0.12–0.54 μg mL^{-1}, respectively. What's more, the precisions of intra-day and inter-day were all below 3.2% and 2.9%, respectively.

3.4.2 Purification and capturing nNOS–PSD-95 uncouplers from SXD by MIL@MIPs-SPE-HPLC

MIL@MIPs were used as sorbents for SPE column to capture nNOS–PSD-95 uncouplers from SXD. The initial extract and active components treated with MIL@MIPs were detected by
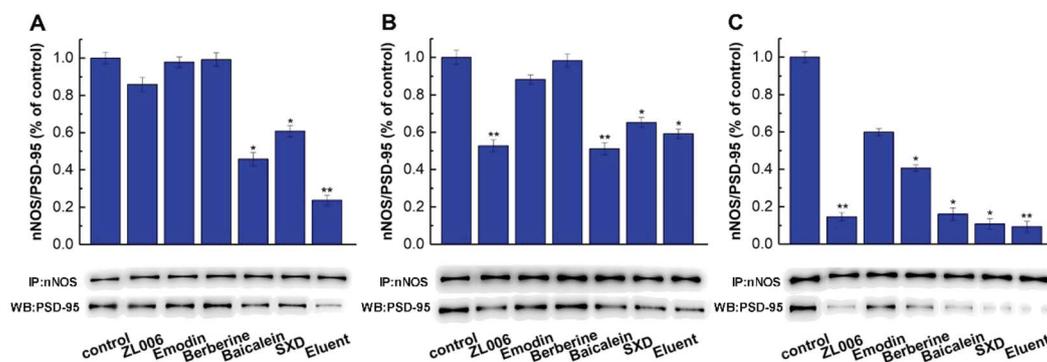

Fig. 7 Uncoupling efficiency assay of ZL006, emodin, baicalein, berberine, SXD and eluent (active components) at 30 μmol L^{-1} (A), 60 μmol L^{-1} (B) and 90 μmol L^{-1} (C) in vitro. Samples were immunoprecipitated by Flag-nNOS antibody (IP) and blots were incubated with PSD-95 antibody (WB). Date is presented as mean ± S.D. *$p < 0.05$, **$p < 0.01$ compared with the control.

HPLC and the results were shown in Fig. 5. It could be seen that active components (the blue curve of Fig. 5A) were much simpler than the initial extract (the red curve of Fig. 5A), which was complicated and diverse. From the chromatograms, we can find that (1) coptisine, (2) baicalin, (3) berberine, (4) emodin-8-O-β-D-glucopyranoside, (5) wogonoside, (6) baicalein, (7) emodin, (8) chrysophanol, and (9) physcion (Fig. 5B) were obtained in the eluent by HPLC-MS and all the nine compounds were then further confirmed by comparing the retention time and molecular weight with standards (Table S5†). As a consequence, we can see that the method established by combining MIL@MIPs-SPE with HPLC has highly selective capacity and is feasible, simple, and time-saving.

3.5 Activity evaluation of active components obtained from SXD

3.5.1 Neuroprotective effect of active components on PC12 cells. PC12 cells were chosen to establish a model of glutamate-induced neuronal injury because they were similar to neuronal apoptosis in ischemic stroke, and MTS cell viability assay was conducted to investigate the neuroprotective effect of active components obtained from SXD. From the initial experiments, DMSO had little effect on PC12 cells when it reached its finial concentration below 0.1% (v/v), therefore it was not employed in the following experiments. Fig. 6A clearly showed that 5 mmol L^{-1} glutamate could lead to about 50% inhibition of PC12 cells and were thus chosen as the optimal condition for the
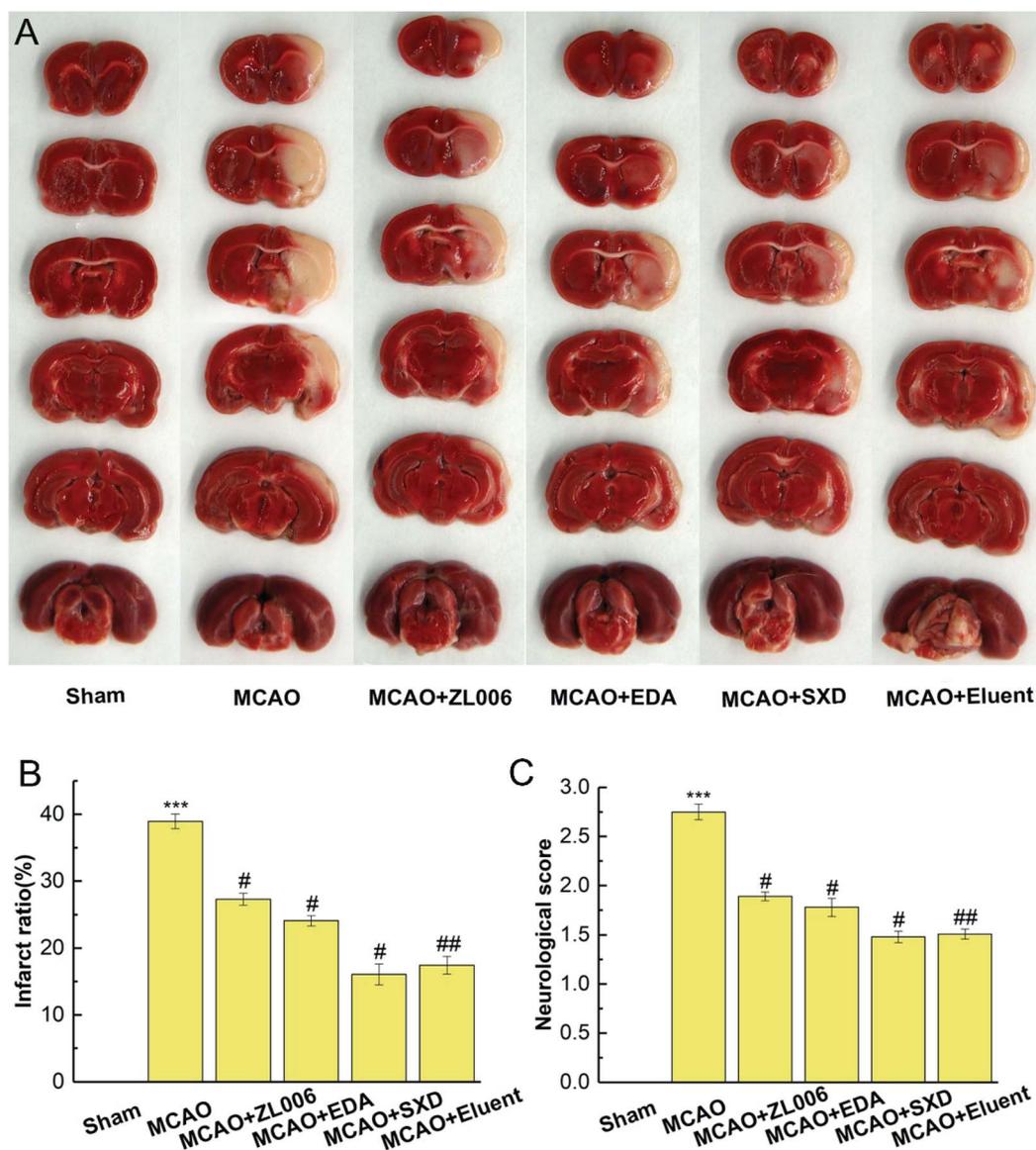

Fig. 8 The effect of ZL006, EDA, SXD and eluent (active components) on treating ischemic stroke *in vivo*. (A) The representative brain slices stained by TTC of the sham-operated group, the MCAO group and the treatment group, (B) the infarct ration of each group, (C) the neurological deficit scores of each group. Date is presented as mean ± S.D. ***$P < 0.001$ compared with the sham-operated group, #$P < 0.05$, ##$P < 0.01$ compared with the MCAO group.

subsequent experiments. From Fig. 6B, we can see that active components exhibited better neuroprotective effect than ZL006 (the positive control compound) at the concentration of 75 μmol L^{-1}, and baicalein was even more efficacious than ZL006 at a low concentration of 15 μmol L^{-1}. The morphological changes of PC12 cells with different treatments were shown in Fig. 6C. Compared with the exuberant and fibriform control cells (Fig. 6C(a)), the cells treated with 5 mmol L^{-1} glutamate (Fig. 6C(b)) became rounded instead of fine dendritic and decreased sharply, while the number of PC12 cells increased apparently, and most of the cells converted to their initial morphology after dealing with 105 μmol L^{-1} active components (Fig. 6C(c)). For further quantitative comparison, EC_{50} values of the compounds on glutamate-injured PC12 cells were evaluated (Table S6†). Consequently, the active components (20.548 μmol L^{-1}) appeared to be better than ZL006 (26.674 μmol L^{-1}).

3.5.2 Uncoupling activity of active components *in vitro*. Co-immunoprecipitation experiment was conducted to evaluate the uncoupling efficiency of active components obtained from SXD. According to the preliminary trials, the experimental concentrations of samples were set as 30 μmol L^{-1}, 60 μmol L^{-1}, and 90 μmol L^{-1}, respectively. As presented in Fig. 7, ZL006 showed obvious ability to block the interaction of nNOS–PSD-95 in a dose-dependent manner within the concentrations of 30–90 μmol L^{-1}. Nevertheless, SXD, active components, and baicalein showed significant uncoupling ability at the concentration of 30 μmol L^{-1} (Fig. 7A). At the concentration of 60 μmol L^{-1}, SXD, active components, and baicalein also had uncoupling capacity but no better than ZL006 (Fig. 7B). However, SXD, active components, baicalein, and berberine showed excellent uncoupling ability at 90 μmol L^{-1}. What is more, the active components even appeared to be more efficacious than ZL006 (Fig. 7C).

3.5.3 Anti-ischemic stroke efficacy of active components *in vivo*. MCAO/R model was applied to investigate the anti-ischemic stroke efficacy of active components obtained from SXD after the MTS research and the co-immunoprecipitation experiment were analyzed comprehensively. Then the neuro-logical deficit scores were evaluated and the infarct ratio was calculated. By comparison, the sham-operated group showed no neurological deficit or infarct, while nearly 40% infarct ratio appeared in the MCAO group. From Fig. 8, both neurological deficit score (1.5) and infarct ratio (17.4%) showed that active components obtained from SXD could reduce the infarct size and alleviate neurological damage and were also superior to ZL006 and EDA, which highly suggested that active components obtained from SXD by MIL@MIPs-SPE-HPLC had potential uncoupling activity and anti-ischemic stroke efficacy.

4. Conclusion

Novel molecularly imprinted polymers based on NH$_2$-MIL-101 (MIL@MIPs) were successfully designed, optimized, and char-acterized, which exhibited large binding capacity, fast kinetics, excellent selectivity, rapid desorption ability, and satisfactory reusability by adsorption performance experiments. Then a model of MIL@MIPs-SPE-HPLC was applied to capture nNOS–

PSD-95 uncouplers from SXD. MTS assay and coimmunopreci-pitation experiment demonstrated that the active components obtained from SXD showed excellent neuroprotective effect and uncoupling activity *in vitro*. At the same time, it could also reduce the infarct size and ameliorate neurological deficits significantly estimated in anti-ischemic stroke assay *in vivo*. Furthermore, this study can provide a scientific basis for the application of SXD and its optimized prescriptions. Meanwhile, it can also provide new ideas and new methods for efficiently capturing nNOS–PSD-95 uncouplers from other nature medicines.

Live subject statement

All animal procedures were performed in accordance with the Guidelines for Care and Use of Laboratory Animals of Nanjing Medical University and experiments were approved by the Animal Ethics Committee of Nanjing Medical University.

Conflicts of interest

There are no conflicts to declare.

Acknowledgements

References

1 B. Chen, G. X. Wang, W. W. Li, W. L. Liu, R. H. Lin, J. Tao, M. Jiang, L. D. Chen and Y. Wang, *Exp. Cell Res.*, 2017, **351**, 163–172.

2 A. S. Ernst, L. I. Böhler, A. M. Hagenston, A. Hoffmann, S. Heiland, C. Sticht, M. Bendszus, M. Hecker, H. Bading, H. H. Marti, T. Korff and R. Kunze, *Acta Neuropathol. Commun.*, 2019, **7**, 15.

3 Q. J. Wu and M. Tymianski, *Mol. Brain*, 2018, **11**, 15.

4 Y. J. Kaneko, J. P. Tuazon, X. M. Ji and C. V. Borlongan, *Cell. Physiol. Biochem.*, 2018, **51**, 1982–1995.

5 A. Bach, S. W. Pedersen, L. A. Dorr, G. Vallon, I. Ripoche, S. Ducki and L. Y. Lian, *Sci. Rep.*, 2015, **5**, 12157.

6 S. F. Mo, G. Y. Liao, J. Yang, M. Y. Wang, Y. Hu, G. N. Lian, L. D. Kong and Y. Zhao, *Brain Res.*, 2016, **1648**, 250–256.

7 S. C. Wu, Y. Yue, H. Tian, L. Tao, Y. T. Wang, J. Xiang, S. Wang and H. Ding, *Neuropharmacology*, 2014, **83**, 107–117.

8 S. K. Florio, C. Loh, S. M. Huang, A. E. Iwamaye, K. F. Kitto, K. W. Fowler, J. A. Treiberg, J. S. Hayflick, J. M. Walker, C. A. Fairbanks and Y. Lai, *Br. J. Pharmacol.*, 2009, **158**, 494–506.

9 L. Zhou, F. Li, H. B. Xu, C. X. Luo, H. Y. Wu, M. M. Zhu, W. Lu, X. Ji, Q. G. Zhou and D. Y. Zhu, *Nat. Med.*, 2010, **16**, 1439–1443.

10 D. Y. Chen, T. Zhao, K. D. Ni, P. Dai, L. Yang, Y. Xu and F. Li, *Bioorg. Med. Chem. Lett.*, 2016, **26**, 2152–2155.

11 X. L. Gu, J. J. Huang, L. Zhang, Y. Zhang, C. Z. Wang, C. H. Sun, D. D. Yao, F. Li, L. N. Chen and C. S. Yuan, *J. Sep. Sci.*, 2017, **40**, 3522–3534.

12 D. D. Yao, L. Zhang, J. J. Huang, C. H. Sun, Y. Zhang, X. L. Gu, C. Z. Wang, F. Li, L. N. Chen and C. S. Yuan, *J. Pharm. Biomed. Anal.*, 2018, **154**, 180–190.

13 J. J. Huang, C. H. Sun, D. D. Yao, C. Z. Wang, L. Zhang, Y. Zhang, L. N. Chen and C. S. Yuan, *J. Mater. Chem. B*, 2018, **6**, 1531–1542.

14 X. Y. Wei, J. H. Tao, X. Cui, S. Jiang, D. W. Qian and J. A. Duan, *J. Chromatogr. B: Anal. Technol. Biomed. Life Sci.*, 2017, **1061**, 248–255.

15 T. Y. Wu, F. R. Chang, J. R. Liou, I. W. Lo, T. C. Chung, L. Y. Lee, C. C. Chi, Y. C. Du, M. H. Wong, S. H. H Juo, C. C. Lee and Y. C. Wu, *Front. Pharmacol.*, 2016, **7**, 374.

16 Y. T. Shih, D. C. Wu, C. M. Liu, Y. C. Yang, I. J. Chen and Y. C. Lo, *J. Ethnopharmacol.*, 2007, **112**, 537–544.

17 S. F. Liou, J. H. Hsu, J. C. Liang, H. J. Ke, I. J. Chen, J. R. Wu and J. L. Yeh, *J. Nat. Med.*, 2012, **66**, 311–320.

18 X. Y. Wei, J. H. Tao, Y. M. Shen, S. W. Xiao, S. Jiang, E. X. Shang, Z. H. Zhu, D. W. Qian and J. N. Duan, *Front. Pharmacol.*, 2018, **9**, 955.

19 K. Lee, B. Kim, H. Hur, K. S. Chinannai, I. Ham and H. Y. Choi, *Chin. J. Integr. Med.*, 2017, DOI: 10.1007/s11655-017-2771-7.

20 Y. S. Wang, R. T. Lin, H. Y. Cheng, S. F. Yang, W. W. Chou and S. H. H. Juo, *J. Ethnopharmacol.*, 2011, **133**, 442–447.

21 J. X. Song, X. Chen, Y. Lyu, W. Zhuang, J. Zhang, L. Gao and X. L. Tong, *Brain and Behavior*, 2019, **9**, e01185.

22 L. Uzun and A. P. F. Turner, *Biosens. Bioelectron.*, 2016, **76**, 131–144.

23 O. S. Ahmad, T. S. Bedwell, C. Esen, A. Garcia-Cruz and S. A. Piletsky, *Trends Biotechnol.*, 2019, **37**, 294–309.

24 R. I. Boysen, *J. Sep. Sci.*, 2019, **42**, 51–71.

25 Z. Z. Wu, D. Y. He, B. Cui and Z. Y. Jin, *Food Chem.*, 2019, **283**, 517–521.

26 C. Li, M. H. Ngai, K. K. Reddy, S. C. Y. Leong, Y. W. Tong and C. L. L. Chai, *Anal. Chim. Acta*, 2019, **1066**, 121–130.

27 W. Shi, S. Q. Zhang, K. B. Li, W. P. Jia and D. M. Han, *Sep. Purif. Technol.*, 2018, **202**, 165–173.

28 Y. C. Lu, M. H. Guo, J. H. Mao, X. H. Xiong, Y. J. Liu and Y. Li, *Ecotoxicol. Environ. Saf.*, 2019, **177**, 66–76.

29 R. Sedghi, B. Heidari and M. Yassari, *J. Colloid Interface Sci.*, 2017, **503**, 47–56.

30 J. Ashley, M. A. Shahbazi, K. Kant, V. A. Chidambara, A. Wolff, D. D. Bang and Y. Sun, *Biosens. Bioelectron.*, 2017, **91**, 606–615.

31 M. D. Attieh, Y. Zhao, A. Elkak, A. Falcimaigne-Cordin and K. Haupt, *Angew. Chem., Int. Ed.*, 2017, **56**, 3339–3343.

32 M. Tatemichi, M. Sakamoto, M. Mizuhata, S. Deki and T. Takeuchi, *J. Am. Chem. Soc.*, 2007, **129**, 10906–10910.

33 T. Guo, Q. L. Deng, G. Z. Fang, D. H. Gu, Y. K. Yang and S. Wang, *Biosens. Bioelectron.*, 2016, **79**, 341–346.

34 M. Khdhayyer, A. F. Bushell, P. M. Budd, M. P. Attfield, D. M. Jiang, A. D. Burrows, E. Esposito, P. Bernardo, M. Monteleone, A. Fuoco, G. Clarizia, F. Bazzarelli, A. Gordano and J. C. Jansen, *Sep. Purif. Technol.*, 2019, **212**, 545–554.

35 K. Qian, Q. L. Deng, G. Z. Fang, J. P. Wang, M. F. Pan, S. Wang and Y. H. Pu, *Biosens. Bioelectron.*, 2016, **79**, 359–363.

36 S. Clauzier, L. N. Ho, M. Pera-Titus, B. Coasne and D. Farrusseng, *J. Am. Chem. Soc.*, 2012, **134**, 17369–17371.

37 X. P. Dai, X. N. Jia, P. Zhao, T. Wang, J. Wang, P. T. Huang, L. He and X. H. Hou, *Talanta*, 2016, **154**, 581–588.

38 H. L. Liu, L. Mu, X. M. Chen, J. Wang, S. Wang and B. G. Sun, *J. Agric. Food Chem.*, 2017, **65**, 986–992.

39 Z. W. Xiao, M. He, B. B. Chen and B. Hu, *Talanta*, 2016, **156**, 126–133.

40 Y. Lin, C. Kong and L. Chen, *RSC Adv.*, 2012, **2**, 6417–6419.